Inorganic Chemistry

Article

pubs.acs.org/IC

Magnetic Order Through Super-Superexchanges in the Polar Magnetoelectric Organic–Inorganic Hybrid $Cr[(D_3N\text{-}(CH_2)_2\text{-}PO_3)(Cl)(D_2O)]$

Gwilherm Nénert,*[,†] Hyun-Joo Koo,[‡] Claire V. Colin,[§] Elvira M. Bauer,*[,∥] Carlo Bellitto,[∥] Clemens Ritter,[†] Guido Righini,[∥] and Myung-Hwan Whangbo[⊥]

[†]Diffraction Group BP 156, Institut Laue-Langevin, 6 rue Jules Horowitz, F-38042 Grenoble Cedex 9, France

[‡]Department of Chemistry and Research Institute of Basic Science, Kyung Hee University, Seoul 130-701, Republic of Korea

[§]Institut Néel, CNRS et Université Joseph Fourier, BP 166, 38042 Grenoble, France

[∥]Istituto di Struttura della Materia-C.N.R. Sez. Montelibretti, via Salaria km 29.300, P.O. Box 10, 00015 Monterotondo (RM), Italy.

[⊥]Department of Chemistry, North Carolina State University, Raleigh, North Carolina 27695-8204, United States

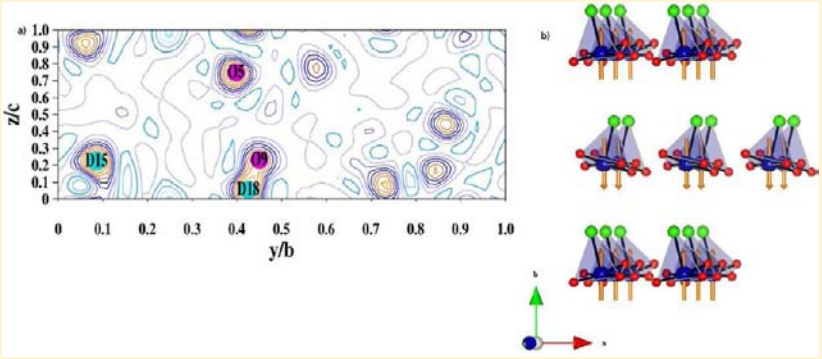

ABSTRACT: The crystal and magnetic structures of the organic–inorganic hybrid compound Cr(II) ammoniumethylphosphonate chloride monohydrate, $Cr[D_3N\text{-}(CH_2)_2\text{-}PO_3)(Cl)(D_2O)]$ (1), have been studied by temperature-dependent neutron powder diffraction and superconducting quantum interference device (SQUID) magnetometry. The compound represents a rare example of a magnetoelectric polar organic–inorganic hybrid solid, containing high spin Cr^{2+} ions ($S = 2$) and is a canted antiferromagnet (weak ferromagnet) below $T_N = 5.5$ K. The neutron powder diffraction pattern recorded at $T = 10$ K, shows that the partially deuterated compound crystallizes in the same non centrosymmetric monoclinic space group $P2_1$ (No. 4) with the following unit-cell parameters: $a = 5.24041(4)$ Å, $b = 13.93113(8)$ Å, $c = 5.26081(4)$ Å, and $\beta = 105.4347(5)°$. Powder neutron diffraction of a partially deuterated sample has enabled us, for the first time, to locate the water molecule. At low temperature, the compound presents a canted antiferromagnetic state characterized by $k = 0$ resulting in the magnetic symmetry $P2_1'$. This symmetry is in agreement with the previously reported large magnetodielectric effect. The crystal structure of (1) can be described as being built up of triangular lattice planes made up of $[Cr(II)O_4Cl]$ square pyramids which are separated by ammonium ethyl groups along the b axis. The transition from paramagnetic to weakly ferromagnetic state results from super-superexchanges only. Surprisingly, while the overall magnetic behavior is antiferromagnetic, the $Cr(II)O_4Cl$ planes are ferromagnetic, and the strongest antiferromagnetic coupling is via the ammonium ethyl groups. Our density functional calculations confirm these aspects of the spin exchange interactions of (1) and that the spin exchange interactions between Cr(II) ions are considerably weak compared with the single-ion anisotropy of Cr^{II}.

INTRODUCTION

Phosphonates containing transition metals have been widely studied because of their potential to serve as ionic exchangers,[1] catalysts,[2] hosts for intercalation compounds,[3] and more recently as magnetic[4] and multifunctional[5] compounds. Molecule-based magnets displaying[6] canted antiferromagnetism, low-dimensional magnetism, polar magnets and porous magnetic solids are getting more and more attention. Quite recently, we were able to prepare and characterize a series of organic–inorganic hybrids based on metal(II) phosphonate, $M^{II}[RPO_3)(H_2O)]$ (M = Cr, Fe, Co and Ni).[7] The crystal structures solved for some of them show that they are lamellar, with alternating inorganic and organic layers along one direction of the unit cell. The inorganic layers consist of M^{II} ions bridged by the oxygen atoms of phosphonate groups, and the resulting metal–oxygen network forms sheets separated one from the other by the organic R group of the ligand. The

Received: August 28, 2012
Published: December 28, 2012

   dx.doi.org/10.1021/ic301874v | *Inorg. Chem.* 2013, 52, 753–760

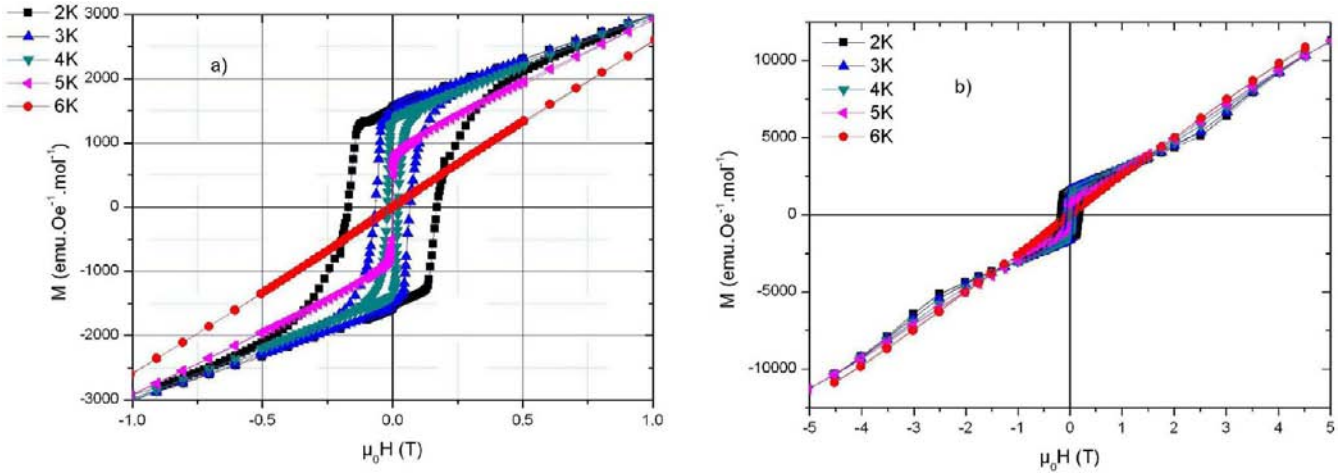

Figure 1. Magnetization of $Cr[(D_3N\text{-}(CH_2)_2\text{-}PO_3)(Cl)(D_2O)]$ as a function of the magnetic field in the temperature range 6 to 2 K. (a) -1 T < H < 1 T and (b) -5 T < H < 5 T.

organic part of the phosphonate $[RPO_3]^{2-}$ can be chemically modified by introducing different functional groups (e.g., the amino groups) to get an organic–inorganic hybrid structure bound by covalent and/or ionic bonds. This enables one to design multifunctional solids, which could be suitable for technological applications.

With this in mind, we designed and prepared the compound $Cr[H_3N\text{-}(CH_2)_2\text{-}PO_3)(Cl)(H_2O)]$ a few years ago,[8] which is a polar layered organic–inorganic hybrid and magnetically orders at low temperature. The rare combination of these two features triggered the investigation of its magnetodielectric properties. There occurs a strong enhancement of the magnetodielectric coupling below T_N, which results from the appearance of the long-range magnetic order.[9] To gain more insight into the magnetic behavior of the title compound below the ordering temperature, we have carried out a high resolution powder neutron diffraction experiment at low temperature, investigated further the magnetic field dependence of the magnetization using superconducting quantum interference device (SQUID) magnetometry, and examined the spin exchange interactions between Cr(II) ions and the single-ion anisotropy of Cr(II) on the basis of first principles density functional theory (DFT) calculations.

EXPERIMENTAL SECTION

Synthesis of Partially Deuterated $Cr[(D_3N\text{-}(CH_2)_2\text{-}PO_3)(Cl)\text{-}(D_2O)]$. A solution of $Cr^{II}Cl_2$ in deuterated water was prepared by dissolving chromium metal (1.0 g, 19 mmol) under inert atmosphere and under mild heating in a Schlenck tube in 15 mL of DCl (2 M, in deuterated water). After 24 h, a blue solution is obtained, which is filtered and transferred under nitrogen in a Schlenk tube containing 2-aminoethylphosphonic acid (1.8 g, 14.4 mmol) and fully deuterated urea (2.6 g, 40.6 mmol). The blue reaction mixture is heated under nitrogen flux for several days at 85–90 °C. During the reaction, a blue microcrystalline precipitate is formed which has been filtered under inert atmosphere, washed with deuterated water, and dried under vacuum. The light-blue crystalline powder was characterized by IR spectroscopy and sealed in a quartz ampule.

SQUID Magnetometry. Static magnetic susceptibility measurements were performed by using a Quantum Design MPMS5 SQUID magnetometer in fields up to 5 T from 300 to 2.0 K. A cellulose capsule was filled with a freshly prepared polycrystalline sample and placed inside a polyethylene straw.

Neutron Powder Diffraction Experiments. Temperature-dependence neutron powder diffraction measurements were performed on the high resolution D1A diffractometer at the Institut Laue Langevin (ILL), Grenoble. In the configuration used, the resolution fwhm of D1A was about 0.3° at 90°. The measurements were carried out at a wavelength of λ = 1.909 Å selected by the (115) reflection of a germanium monochromator. The neutron detection was performed with a set of 25 ^{3}He counting tubes spaced by 6°. Diffraction patterns over the whole 2θ range 0°–140° were obtained by scanning in steps of 0.1° at 2 and 10 K. The sample was sealed in a cylindrical vanadium can and loaded inside an ILL orange cryostat. Diffraction data analysis was done using the FULLPROF refinement package.[10]

RESULTS AND DISCUSSION

Magnetic Properties. Previous magnetic susceptibility measurements of undeuterated $Cr[(H_3N(CH_2)_2PO_3)\text{-}(Cl)\cdot H_2O]$ showed the compound to be paramagnetic above 10 K obeying the Curie–Weiss law with a Curie constant C = 2.716 cm^3 K mol^{-1} and the Weiss constant $\theta = -2.2$ K.[8c] The corresponding effective magnetic moment of 4.7 μ_B is consistent with the presence of a Cr^{II} ion in the d^4 (S = 2) high-spin configuration (spin-only value 4.9 μ_B). Below about 6 K, a sharp increase in the product χT was observed with a maximum of ~40 cm^3 K mol^{-1} (for an applied field of 100 Oe) at $T \approx 5$ K. The field-cooled magnetization (M_{fc}) and zero-field-cooled (M_{zfc}) magnetizations, measured with an applied magnetic field of 25 Oe in the temperature range of 4.2–10 K, show that the M_{fc} vs T plot increases rapidly below T = 5.7 K while the M_{zfc} vs T plot has a narrow peak with maximum around 5 K. This led to the conclusion that $Cr[(H_3N\text{-}(CH_2)_2PO_3)(Cl)\cdot H_2O]$ behaves as a canted antiferromagnet below T_N = 5.5 K. With the aim of studying in detail the magnetic ordered state, we measured several hysteresis loops between 2 and 6 K. Below the critical temperature T_N = 5.5 K (see Figure 1), the hysteresis loops are similar in shape. The weak ferromagnetic component M_F was determined from the extrapolation to zero field of the linear part of the magnetization at higher applied magnetic fields. The temperature dependence of M_F is presented in Figure 2. As $T \rightarrow 0$ K, the value of M_F approaches 1600 emu Oe^{-1} mol^{-1}, which is equivalent to ~0.3 μ_B per formula unit (f.u.), and drops to zero at T_N. At 2 K, the coercive field is about 0.17 T, and the remanent magnetization M_r about 1500 emu Oe^{-1} mol^{-1}. The canting angle α is estimated to be about 4° based on the equation $\alpha = \sin^{-1}(M_r/M_s)$, where M_s is $4N_A\beta$, N_A the Avogadro's number, and β the Bohr magneton).[11]

dx.doi.org/10.1021/ic301874v | Inorg. Chem. 2013, 52, 753–760

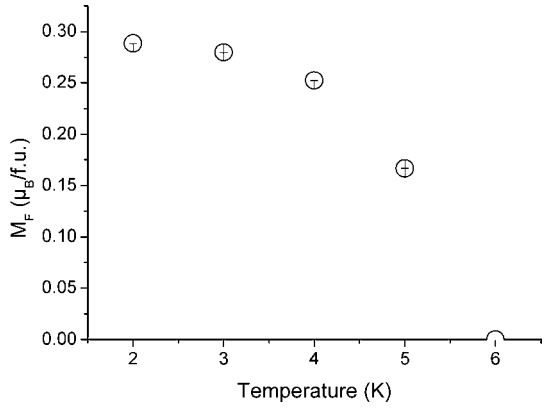

Figure 2. Weak ferromagnetic component, M_F as determined from the magnetization measurement as a function of temperature.

The plot M versus H, measured at T = 6.0 K, (see Figure 1) is linear, thus indicating a paramagnetic state at temperatures above 6 K. The phase change from the paramagnetic to a weakly ferromagnetic state occurs without any noticeable intermediate antiferromagnetic state. This can be ascribed to the predominance of the single-ion anisotropy D over the exchange coupling J/k_B, as confirmed by our evaluation of the spin exchange and the single-ion anisotropy (see below). In addition, a magnetic field induced phase is observed below the magnetic ordering temperature, with the critical field ~3 T at 2 K.

Neutron Powder Diffraction Studies. *Crystal Structure.* The neutron powder diffraction pattern of $Cr[(D_3N\text{-}(CH_2)_2\text{-}PO_3)(Cl)(D_2O)]$ at 10 K was first refined using the structural model determined from the room temperature X-ray diffraction. This did not give a good fit of the intensities since the hydrogen atoms of the water molecule could not be located from the X-ray single crystal study. To facilitate the location of these missing hydrogen atoms a partially deuterated sample was used in the neutron study. The two deuterium atoms bonded to the oxygen of the water molecule were then visible in the Fourier difference map (see Figure 3) which was calculated from the refinement using the X-ray model and the observed neutron data.

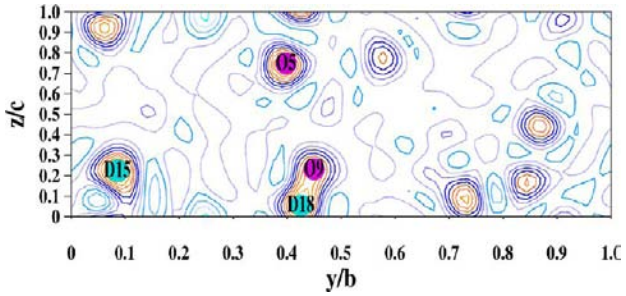

Figure 3. Fourier difference map showing the location of the deteurium atoms forming the water molecule (atom D18 connected to O9).

The refinement of the 10 K data was done with FullProf[10] using the monoclinic space group $P2_1$ with the unit-cell parameters: a = 5.24041(4) Å, b = 13.93113(8) Å, c = 5.26081(4) Å, and β = 105.4347(5)°. The observed, calculated, and difference patterns of the final refinement of the nuclear structure are reported in Figure 4. In Table 1 are reported the atomic coordinates of $Cr[(D_3N\text{-}(CH_2)_2\text{-}PO_3)(Cl)(D_2O)]$ including those of the deuterium atoms. Figure 5 shows the layered crystal structure of $Cr[(D_3N\text{-}(CH_2)_2\text{-}PO_3)(Cl)(D_2O)]$. The crystal structure is lamellar, made up of alternating inorganic and organic layers along the polar b-axis. The inorganic layer is formed by $[Cr(II)O_4Cl]$ square pyramids made up of three oxygens from the phosphonates, one oxygen from the water molecule, and a Cl^- ion at the apical position.

The refinement of the powder neutron diffraction data enables us to identify the positions of the deuterium atoms of the water molecule. In Table 1 the oxygen atom of the water molecule is referred to as O9. There are several oxygen deuterium bonds in the structure. The O9−D18 bond is 0.989(10) Å and is parallel to the c axis while the oxygen donor···deuterium acceptor bond D18···O5 is 1.774(10) Å. The other oxygen−deuterium bonds are roughly perpendicular to the c axis thus forming a pseudosquare lattice perpendicular to the polar b axis. These bonds are respectively 0.990(10) Å for the D19−O9 bond, and 1.844(10) Å for the D19···O6 bond.

Magnetic Structure. To investigate the nature of the magnetic ground state and the origin of the large magnetodielectric effect reported in this material,[9] neutron powder data were collected at 2 K, below the Néel temperature ($T_N \approx 5.5$ K). The observed diffraction patterns below and above T_N are shown in Figure 6. No new diffraction peaks appear in the 2 K pattern but the (110) and (011) reflections increase significantly in intensity. This confirms the appearance of a long-range magnetic ordering below $T_N \approx 5.5$ K in good agreement with previous reports[8c,9] and our magnetization data. These magnetic reflections can be indexed using a propagation magnetic wave-vector $\mathbf{k} = \mathbf{0}$.

The possible magnetic structures compatible with the symmetry of $Cr[(D_3N\text{-}(CH_2)_2\text{-}PO_3)(Cl)(D_2O)]$ are determined by following the representation analysis technique described by Bertaut.[12] For the propagation vector $\mathbf{k} = \mathbf{0}$, the little group G_k, formed by those elements of the space group that leave $\mathbf{k}$ invariant, coincides with the space group $P2_1$. For $\mathbf{k} = \mathbf{0}$, the irreducible representations of the group G_k are those shown in Table 2.

A representation Γ is constructed with the Fourier components $\mathbf{m}_k$ corresponding to the Cr atoms of the Wyckoff position 2a. The Cr atoms at the site 2a are denoted as (1) (x, y, z) and (2) ($-x$, y + 1/2, $-z$). The decomposition of the representation Γ in terms of the irreducible representations Γ_j is for the 2a site,

$$\Gamma(2a) = 3\Gamma_1 + 3\Gamma_2$$

We have two Cr^{2+} ions per unit cell. Consequently, there are only two different possible couplings between them: one ferromagnetic configuration ($\mathbf{M} = \mathbf{S}_1 + \mathbf{S}_2$) and one antiferromagnetic configuration ($\mathbf{L} = \mathbf{S}_1 - \mathbf{S}_2$). The different basis vectors associated with each irreducible representation and calculated by using the projection operator technique implemented in BasIreps[14] are presented in Table 3.

We have tested both models for the refinements. The best fit to the data could be obtained only for the model described by the irreducible representation Γ_2 (R_{mag} = 4.15%). During the refinement, we noticed that there were some strong correlations between the atomic positions and the magnetic moment value. This usually resulted in physically unreasonable values of the magnetic moment. Consequently we have fixed the atomic coordinates to the values determined at 10 K and

dx.doi.org/10.1021/ic301874v | Inorg. Chem. 2013, 52, 753−760

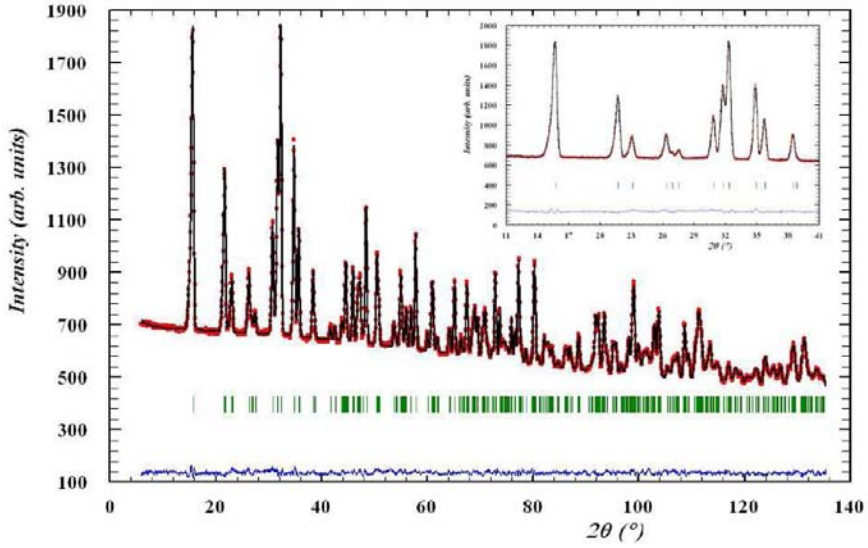

Figure 4. Observed, calculated, and difference diffraction profile patterns for a powder sample of $Cr[(D_3N\text{-}(CH_2)_2\text{-}PO_3)(Cl)(D_2O)]$ collected at 10 K. Inset: zoomed-in view for the low angle region.

Table 1. Atomic Coordinates of $Cr[(D_3N\text{-}(CH_2)_2\text{-}PO_3)(Cl)(D_2O)]$ Determined from the Powder Neutron Diffraction at 10 K[a]

atom	x	y	z	U_{iso}
Cr1	0.5540(18)	0.3109(7)	0.434(2)	0.0153(20)
P2	0.1290(12)	0.2571(4)	0.8126(14)	0.0101(17)
Cl3	0.4575(6)	0.5(-)	0.5223(6)	0.0103(8)
O4	0.2835(9)	0.3106(5)	0.0637(10)	0.0102(14)
O5	0.8412(10)	0.2965(5)	0.7494(10)	0.0155(17)
O6	0.2530(9)	0.2692(4)	0.5864(10)	0.0142(17)
C7	0.1123(10)	0.1309(3)	0.8802(11)	0.0058(10)
C8	0.9496(13)	0.1096(3)	0.0633(13)	0.0107(12)
O9	0.8161(12)	0.3532(4)	0.2411(12)	0.0158(15)
N10	0.9312(9)	0.0086(3)	0.1102(8)	0.0154(8)
H11	0.0235(19)	0.0990(9)	0.693(2)	0.029(3)
H12	0.3263(19)	0.1039(10)	0.9548(18)	0.035(3)
H13	0.748(2)	0.1420(10)	−0.007(2)	0.036(4)
H14	0.025(2)	0.1367(9)	0.267(3)	0.036(3)
D15	0.8087(11)	−0.0102(5)	0.2279(12)	0.0307(16)
D16	0.1162(11)	−0.0197(5)	0.2014(12)	0.0231(14)
D17	0.8611(12)	−0.0307(5)	0.9452(12)	0.0296(14)
D18	0.7873(10)	0.3301(5)	0.0553(10)	0.0263(14)
D19	0.9954(11)	0.3285(5)	0.3288(10)	0.0286(15)

[a]Space group: $P12_11$ (#4), unit-cell parameters: a = 5.24041(4) Å, b = 13.93113(8) Å, c = 5.26081(4) Å, and β = 105.4347(5)°. Statistics: R_p: 5.89%, R_{wp}: 5.03%, R_{exp}: 3.96% χ^2: 1.61. The y coordinate of Cl3 was fixed to define the origin of the polar symmetry.

refined only the peak shape, magnetic structure, cell parameters, and background. We show in Figure 7, the observed, calculated, and difference patterns of the refinement that we have carried out. A representation of the magnetic structure is given in Figure 8. The magnetic structure consists of triangular ferromagnetic lattices parallel to the ac-planes that are coupled antiferromagnetically along the polar b axis.

From Table 3, we see that the two magnetic structures allowed by symmetry permit a weak ferromagnetic component which is either along the b-axis or within the (ac) plane. This is in agreement with our SQUID data and the ones published previously.[8c] The deduced magnetic moment from the refinement is $\mu(Cr^{2+})$ = 4.07(4) μ_B. Despite that a weak ferromagnetic behavior is observed in the magnetization data and allowed by symmetry, no ferromagnetic component could be refined with the neutron diffraction data. This is not unexpected in the light of the weak ferromagnetic moment which results in a small canting angle α (see Figure 2, $M_F \approx$ 1600 emu mol^{-1} ($\sim$ 0.3 μ_B/f.u.), $\alpha \approx 4°$). The symmetry of the magnetically ordered phase is $P2_1$, which allows for a linear magnetoelectric effect.[15] This probably explains the large magnetodielectric coupling that we observed previously.[9]

Theoretical Analysis of the Spin Exchange and Spin Orientation. One can notice clearly from the crystal structure representation given in Figure 5 that the spin exchange interactions between the $[Cr(II)O_3O_wCl]$ adjacent subunits is mediated by the phosphonate groups. Consequently the magnetic interactions consist of super-superexchanges (SSE) only. This characteristic of the title compound, though not unique, is sufficiently rare to be highlighted. It has been shown that SSE interactions can be stronger than superexchange paths.[16] A good illustration is the vanadyl vanadate salt $(Sr,Pb)_2(VO)(VO_4)_2$ with S = 1/2 chains where the V^{4+}-V^{4+} SSE through VO_4 groups is 2 orders of magnitude greater than V−O−V superexchange.[17] We show in Figure 9 a representation of the magnetic lattice within the ac-plane, which forms a triangular lattice. This lattice is not likely to be magnetically frustrated, because our neutron diffraction study shows that the spins are ferromagnetically coupled. This is confirmed by the theoretical analysis.

We evaluate the four spin exchanges J_1−J_4 of $Cr[H_3N\text{-}(CH_2)_2\text{-}PO_3)(Cl)(H_2O)]$, depicted in Figure 10, on the basis of DFT electronic structure calculations for the five ordered spin states shown in Figure 11. Our spin-polarized DFT calculations employed the projected augmented-wave method encoded in the Vienna ab initio simulation package,[18] the generalized gradient approximation (GGA) for the exchange-correlation correction,[19] the plane wave cut off energy of 550 eV, a set of 4 × 2 × 4 k-points, and the threshold 10^{-6} eV for self-consistent-field energy convergence. The strong electron correlation associated with the Cr 3d states was taken care of by performing GGA plus on-site repulsion (GGA+U) calcula-

dx.doi.org/10.1021/ic301874v | Inorg. Chem. 2013, 52, 753−760

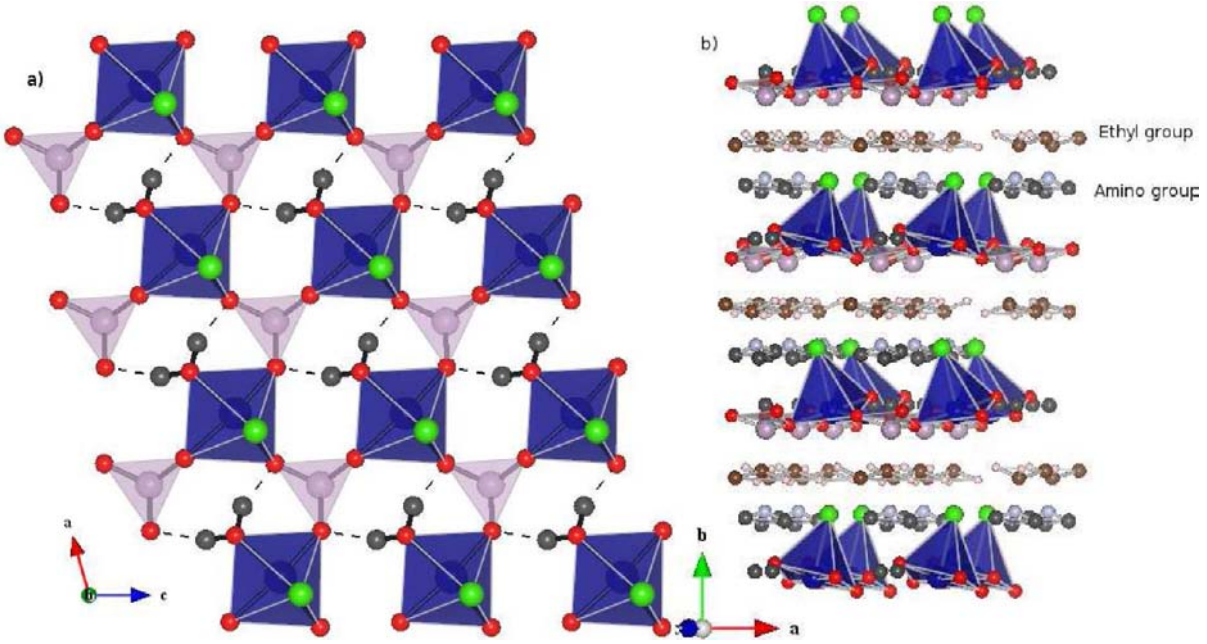

Figure 5. Polyhedral views of the crystal structure of $Cr[(D_3N\text{-}(CH_2)_2\text{-}PO_3)(Cl)(D_2O)]$. (a) The inorganic layer made of CrO_4Cl and phosphonate PO_3 group parallel to the *ac* plane and (b) the stacking of the inorganic and organic layers along the *b*-direction. In panel a, the D−O bonds are represented by solid lines, and the D···O bonds by dashed lines.

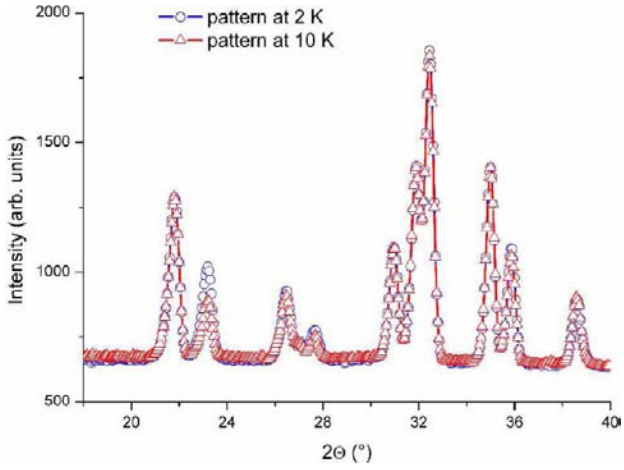

Figure 6. Neutron-powder diffraction patterns of $Cr[(D_3N\text{-}(CH_2)_2\text{-}PO_3)(Cl)(D_2O)]$ collected on the D1A diffractometer at 2 K (circles) and at 10 K (triangles).

Table 2. Irreducible Representations of the Space Group $P2_1$ for k = 0[a]

	h_1	h_3/τ
Γ_1	1	1
Γ_2	1	−1

[a]The symmetry elements are written according to Kovalev's notation,[13] τ = (0,1/2, 0).

Table 3. Basis Vectors for the Atoms of the 2*a* Wyckoff Position

	x	*y*	*z*
Γ_1	L_x	M_y	L_z
Γ_2	M_x	L_y	M_z

tions[20] with U = 3 and 4 eV. The relative energies of the five spin ordered states obtained from the GGA+U calculations with U = 3 and 4 eV are summarized in Figure 11.

To extract the values of the spin exchange parameters J_1−J_4, we express the energies of the ordered spin states in terms of the spin Hamiltonian $\hat{H} = -\sum_{i<j} J_{ij}\,\hat{S}_i\cdot\hat{S}_j$, where J_{ij} (= J_1, J_2, J_3, J_4) refers to the spin exchange parameter for the spin sites *i* and *j*. By applying the energy expressions obtained for spin dimers with N unpaired spins per spin site (in the present case, N = 4),[21] the total spin exchange energies per eight FUs are written as

$$E_{FM} = (-8J_1 - 8J_2 - 8J_3 - 8J_4)(N^2/4)$$

$$E_{AF1} = (-8J_1 - 8J_2 - 8J_3 + 8J_4)(N^2/4)$$

$$E_{AF2} = (+8J_1 - 8J_2 + 8J_3 - 8J_4)(N^2/4)$$

$$E_{AF3} = (+8J_1 + 8J_2 - 8J_3 - 8J_4)(N^2/4)$$

$$E_{AF4} = (-8J_1 + 8J_2 + 8J_3 - 8J_4)(N^2/4)$$

Thus, by equating the relative energies of the ordered spin states from the GGA+U calculations to the corresponding energy differences from the total spin exchange energies, we obtain the values of J_1−J_4 listed in Table 4. All three intralayer spin exchanges are FM, while the interlayer spin exchange is AFM. This result is consistent with the observed magnetic structure of $Cr[H_3N\text{-}(CH_2)_2\text{-}PO_3)(Cl)(H_2O)]$.

Finally, we examine the preferred Cr^{2+} (S = 2) spin orientation in $Cr[H_3N\text{-}(CH_2)_2\text{-}PO_3)(Cl)(H_2O)]$ by performing GGA+U plus spin−orbit coupling (SOC) calculations for the magnetic ground state. Our GGA+U+SOC calculations show that the spin orientation parallel to the *b*-axis (||b) is more stable than that parallel to the *a*-axis (||a) (by 3.1 and 2.7 K/FU from the calculations with U = 3 and 4 eV, respectively), in agreement with our observation. We note that the single-ion

dx.doi.org/10.1021/ic301874v | *Inorg. Chem.* 2013, 52, 753−760

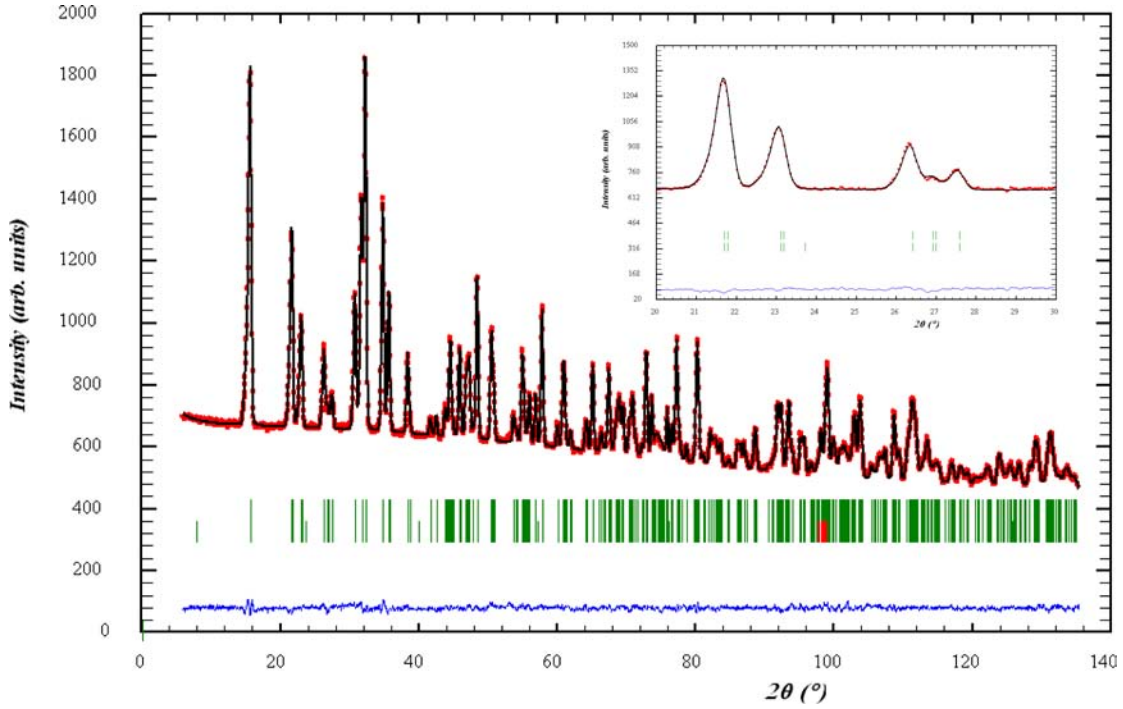

Figure 7. Observed, calculated, and difference diffraction profile patterns for a powder sample of $Cr[(D_3N\text{-}(CH_2)_2\text{-}PO_3)(Cl)(D_2O)]$ collected at 2 K. The inset shows a zoomed-in view of the main magnetic contribution at low angles. Cell parameters: a = 5.24059(4) Å, b = 13.92998(8) Å, c = 5.26100(4) Å, and β = 105.4356(5)°. R_p: 5.73%, R_{wp}: 4.88%, R_{exp}: 3.94% χ^2: 1.54.

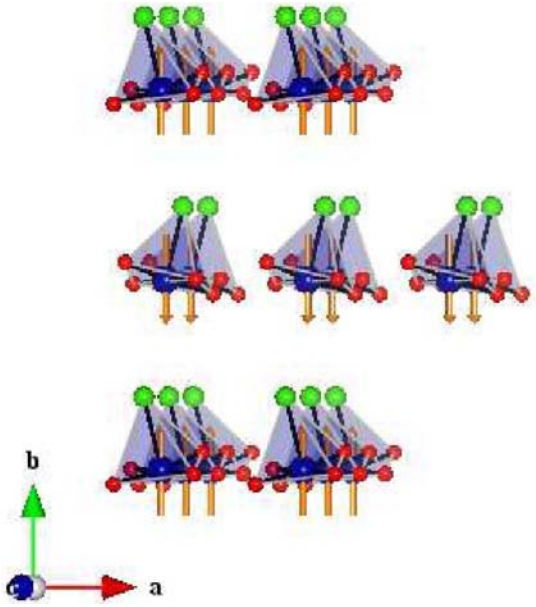

Figure 8. Representation of the antiferromagnetic structure as determined from the powder neutron data at 2 K. The magnetic moment is oriented along the b axis and $\mu(Cr^{2+})$ = 4.07(4) μ_B The magnetic coupling is ferromagnetic within the layers in the (ac) plane and antiferromagnetic between the layers along the b axis.

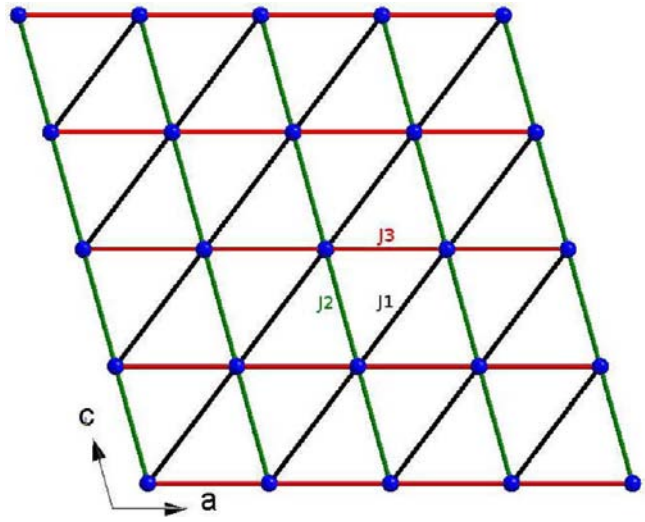

Figure 9. Representation of the super-superexchange paths within the (ac) plane (within the inorganic $Cr(II)O_3O_wCl$ phosphonate layers).

anisotropy is substantially stronger than the strongest spin exchange (3.1 vs 1.3 K and 2.7 vs 1.9 K from the calculations with U = 3 and 4 eV, respectively). As already mentioned, this accounts for why the phase change from the paramagnetic to a weakly ferromagnetic state occurs without any noticeable intermediate antiferromagnetic state.

CONCLUSION

The partially deuterated Cr(II) ammoniumethylphosphonate chloride monohydrate $Cr[D_3N\text{-}(CH_2)_2\text{-}PO_3)(Cl)(D_2O)]$ has been studied by neutron powder diffraction and magnetization measurements down to 2 K. The neutron diffraction pattern recorded at 10 K has enabled us to determine the position of the hydrogen atoms of the water molecule and hence clarify the crystal structure of this polar material. Below the Néel temperature T_N = 5.5 K, a commensurate canted antiferromagnetic structure is observed. The determined magnetoelectric symmetry $P2_1'$ can explain the strong magnetodielectric coupling observed in this material and the weak ferromagnetic

dx.doi.org/10.1021/ic301874v | Inorg. Chem. 2013, 52, 753−760

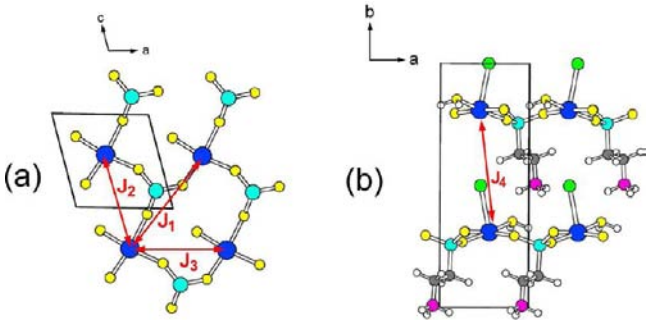

Figure 10. (a) Three spin exchange paths J_1–J_3 within the $CrPO_3$ layer of $Cr[(D_3N\text{-}(CH_2)_2\text{-}PO_3)(Cl)(D_2O)]$, and (b) the interlayer exchange J_4 in $Cr[(D_3N\text{-}(CH_2)_2\text{-}PO_3)(Cl)(D_2O)]$. The blue, cyan, yellow, green, gray, pink, and white circles indicate Cr, P, O, Cl, C, N, and H atoms, respectively.

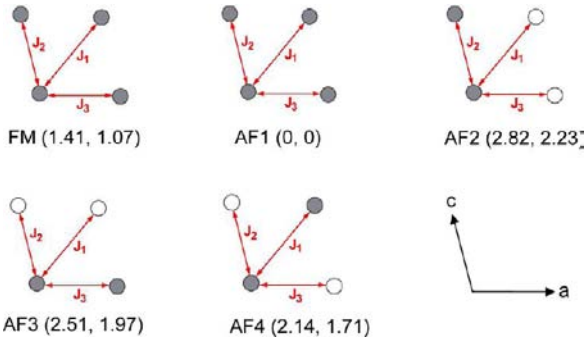

Figure 11. Five ordered spin states used to extract the four spin exchange parameters J_1–J_4. The spin exchange path J_4 between the layers is antiferromagnetic for the AF1 state and ferromagnetic for all other states, FM, AF2, AF3, and AF4. The numbers in each parentheses from left to right refer to the relative energies (in meV/FU) obtained from GGA+U calculations with U = 3 and 4 eV, respectively.

Table 4. Spin Exchange Parameters (in K) Obtained from GGA+U Calculations

	J_1/k_B	J_2/k_B	J_3/k_B	J_4/k_B
U = 3 eV	1.29	0.57	0.75	−2.04
U = 4 eV	1.93	0.46	0.65	−1.56

component of 0.3 μ_B. Our theoretical analysis based on first-principles DFT calculations confirms the presence of ferromagnetic triangular lattice planes coupled antiferromagnetically along the b polar axis, and shows that the spin exchange interactions between Cr(II) ions are considerably weak compared with the single-ion anisotropy of Cr^{II}. The latter explains why the phase change of $Cr[D_3N\text{-}(CH_2)_2\text{-}PO_3)(Cl)(D_2O)]$ from the paramagnetic to a weakly ferromagnetic state occurs without any noticeable intermediate antiferromagnetic state.

AUTHOR INFORMATION

Corresponding Author

*E-mail: nenert@ill.eu (G.N.), Elvira.Bauer@ism.cnr.it (E.M.B.).

Notes

The authors declare no competing financial interest.

ACKNOWLEDGMENTS

This work was supported by the Consiglio Nazionale delle Ricerche (Italy). EU-COST D35 is also acknowledged for support. C.V.C would like to thank B. Canals for useful discussions.

REFERENCES

(1) (a) Alberti, G. In *Comprehensive Supramolecular Chemistry*; Lehn, J. M., Ed.; Pergamon Press: Oxford, U.K., 1996; Vol. 7, pp 151–185; (b) Ma, T.-Y.; Liu, L.; Deng, Q.-F.; Lin, X.-Z.; Yuan, Z.-Y. *Chem. Commun.* **2011**, *47*, 6015–6017.

(2) Clearfield, A. *Prog. Inorg. Chem.* **1998**, *47*, 371–510.

(3) Zhang, B.; Clearfied, A. *J. Am .Chem. Soc* **1997**, *119*, 2751–2752.

(4) (a) Carling, S. G.; Day, P.; Visser, D.; Kremer, R. K. J. *Solid State Chem.* **1993**, *106*, 111–119. (b) For a review see for example (c) Bellitto, C. In *Magnetism: Molecules to Materials*; Miller, J. S., Drillon, M., Eds.; Wiley-VCH: Weiheim, Germany, 2001; Vol. 2, pp 425–456. (d) Mingotaud, C.; Delhaes, P.; Meisel, M. W.; Talham, D. R. In *Magnetism: Molecules to Materials*; Miller, J. S., Drillon, M., Eds.; Wiley-VCH: Weiheim, Germany, 2001; Vol. 2, pp 457–484.

(5) Zhang, L.; Clérac, R.; Heijboer, P.; Schmitt, W. *Angew. Chem., Int. Ed.* **2012**, *51*, 3007–3011. Colodrero, R. M. P.; Olivera-Pastor, P.; Losilla, E. R.; Hernández-Alonso, D.; Aranda, M. A. G.; Leon-Reina, L.; Rius, J.; Demadis, K. D.; Moreau, B.; Villemin, D.; Palomino, M.; Rey, F.; Cabeza, A. *Inorg. Chem.* **2012**, *51*, 7689–7698. Perry, H. P.; Gagnon, K. J.; Law, J.; Tea, S.; Clearfield, A. *Dalton Trans.* **2012**, *41*, 3985.

(6) See for example the series *Magnetism: Molecules to Materials*; Miller, J. S., Drillon, M., Eds.; Wiley-VCH: Weiheim, Germany, 2001; Vols. 1–5.

(7) (a) Bellitto, C.; Federici, F.; Ibrahim, S. A.; Mahmoud, M. R. *1998 MRS Fall Meetings Proc.* **1999**, *547*, 487–492. (b) Altomare, A.; Bellitto, C.; Ibrahim, S. A.; Mahmoud, R. F.; Rizzi, R. *J. Chem. Soc., Dalton Trans.* **2000**, 3913–3919. (c) Altomare, A.; Bellitto, C.; Ibrahim, S. A.; Rizzi, R. *Inorg. Chem.* **2000**, *39*, 1803–1808. (d) Bellitto, C.; Colapietro, M.; Caschera, D.; Federici, F.; Portalone, G. *Inorg. Chem.* **2002**, *41*, 709–714. (e) Bellitto, C.; Bauer, E. M.; Ibrahim, S. A.; Mahmoud, R. F.; Righini, G. *Chem.—Eur. J.* **2003**, *6*, 1324–1331.

(8) (a) Bellitto, C.; Federici, F.; Ibrahim, S. A. *Chem. Commun.* **1996**, 759–760. (b) Bellitto, C.; Federici, F.; Ibrahim, S. A. *Chem. Mater.* **1998**, *10*, 1076–1082. (c) Bauer, E. M.; Bellitto, C.; Colapietro, M.; Portalone, G.; Righini, G. *Inorg. Chem.* **2003**, *42*, 6345–6351.

(9) Nénert, G.; Adem, U.; Bauer, E. M.; Bellitto, C.; Palstra, T. T.; Righini, G. *Phys. Rev.* **2008**, *B78*, 54443(5).

(10) Rodríguez-Carvajal, J. *Phys. B* **1993**, *192*, 55–69.

(11) Carlin, R. L. *Magnetochemistry*; Springer-Verlag: Berlin, Germany, 1986, Kahn, O. *Molecular Magnetism*; VCH: Weinheim, Germany, 1993.

(12) Bertaut, E. F. In *Magnetism*; Rado, G. T., Suhl, H., Eds.; Academic: New York, 1963; Vol. *III*, Chapter 4.

(13) Kovalev, O. V. In *Representations of the Crystallographic Space Groups: Irreducible Representations, Induced Representations and Corepresentations*; Stokes, H. T., Hatch, D. M., Eds.; Gordon and Breach: Amsterdam, The Netherlands, 1993.

(14) J. Rodríguez-Carvajal, BasIreps: A program for calculating irreducible representations of space groups and basis functions for axial and polar vector properties (see http://www.ill.eu/sites/fullprof/php/programsfa7c.html?pagina=GBasireps).

(15) *International Tables for Crystallography Vol. D, Physical Properties of Crystals*; Authier, A., Ed.; Kluwer Academic: Dordrecht, The Netherlands, 2003.

(16) Whangbo, M.-H.; Koo, H.-J.; Dai, D. *J. Solid State Chem.* **2003**, *176*, 417–481.

(17) Mentré, O.; Dhaussy, A. C.; Abraham, F.; Steinfink, H. *J. Solid State Chem.* **1998**, *140*, 417–427. Mentré, O.; Dhaussy, A. C.; Abraham, F.; Suard, E.; Steinfink, H. *Chem. Mater.* **1999**, *11*, 2408–2416. Schmidt, B.; Yushankhai, Y.; Siurakshina, L.; Thalmeier, P. *Eur. Phys. J. B* **2003**, *32*, 43–47.

(18) (a) Kresse, G.; Hafner, J. *Phys. Rev. B* **1993**, *62*, 558−561. (b) Kresse, G.; Furthmüller, J. *Comput. Mater. Sci.* **1996**, *6*, 15−50. (c) Kresse, G.; Furthmüller, J. *Phys. Rev. B* **1996**, *54*, 11169−11186.
(19) Perdew, J. P.; Burke, S.; Ernzerhof, M. *Phys. Rev. Lett.* **1996**, *77*, 3865−3868.
(20) Dudarev, S. L.; Botton, G. A.; Savrasov, S. Y.; Humphreys, C. J.; Sutton, A. P. *Phys. Rev. B* **1998**, *57*, 1505−1509.
(21) (a) Dai, D.; Whangbo, M.-H. *J. Chem. Phys.* **2001**, *114*, 2887−2893. (b) Dai, D.; Whangbo, M.-H. *J. Chem. Phys.* **2003**, *118*, 29−39.